Published in final edited form as:
Mol Imaging Biol. 2014 April ; 16(2): 284–292. doi:10.1007/s11307-013-0676-1.

Comparison of PET Imaging with ^{64}Cu-Liposomes and ^{18}F-FDG in the 7,12-Dimethylbenz[a]anthracene (DMBA)-Induced Hamster Buccal Pouch Model of Oral Dysplasia and Squamous Cell Carcinoma

Lisa M. Mahakian[1], **D. Gregory Farwell**[2], **Hua Zhang**[1], **Jai Woong Seo**[1], **Brian Poirier**[3], **Steven P. Tinling**[4], **Alaa M. Afify**[3], **Eric M. Haynam**[1], **David Shaye**[2], and **Katherine W. Ferrara**[1]

[1]Department of Biomedical Engineering, University of California, Davis, 451 Health Sciences Drive, Davis, CA 95616, USA

[2]Department of Otolaryngology-Head and Neck Surgery, University of California, Davis, 2521 Stockton Blvd Suite 7200, Sacramento, CA 95817, USA

[3]Department of Medical Pathology and Laboratory Medicine, University of California, Davis, 4400 V Street, Sacramento, CA 95817, USA

[4]Department of Otolaryngology-Research Laboratories, University of California, Davis, 1515 Newton Court Room 211, Davis, CA 95618, USA

Abstract

Purpose—Currently, 2-deoxy-2-[^{18}F]fluoro-D-glucose (^{18}F-FDG) is the gold standard radiotracer for staging of head and neck cancer; however, the low sensitivity of this tracer can impede detection of early lesions. ^{64}Cu-liposomes accumulate in various cancers and provide both a sensitive tracer and an indication of the biodistribution of nanotherapeutics. Here, the accumulation of ^{64}Cu-liposomes in early and established cancers is assessed and compared with ^{18}F-FDG in a head and neck cancer model.

Methods—Lesions ranging from mild dysplasia to squamous cell carcinoma were induced in a hamster model of head and neck cancer by topical application of 7,12-dimethylbenz[a]anthracene to the buccal pouch. The hamsters were imaged with micro-positron emission tomography using ^{18}F-FDG and ^{64}Cu-liposomes.

Results—At 24 h postinjection, ^{64}Cu-liposome accumulation exceeded the accumulation of ^{18}F-FDG in every pathologic grade. The lesion-to-cheek pouch (background) ratio and lesion-to-brain ratio were also higher for ^{64}Cu-liposomes than for ^{18}F-FDG.

Conclusion—Imaging of a nanotracer such as ^{64}Cu-liposomes can improve the visualization of head and neck tumors. Accumulation of liposomal particles in head and neck tumors over various pathologic grades averaged 3.5 %ID/cc demonstrating the potential for liposomal therapy with targeted chemotherapeutic agents.

Correspondence to: Katherine W. Ferrara; kwferrara@ucdavis.edu.

Electronic supplementary material The online version of this article (doi:10.1007/s11307-013-0676-1) contains supplementary material, which is available to authorized users.

Conflict of Interest. The authors declare that they have no conflict of interest.

Keywords

Liposomes; Head and neck cancer; Positron emission tomography

Introduction

Cancers of the head and neck are the sixth most common cancer type worldwide and account for nearly 2.3 % of all cancers in the USA [1, 2]. Oral squamous cell carcinoma (SCC) represents approximately 90 % of cancerous lesions that develop in the oral cavity and is often associated with poor prognosis due to advanced stage of presentation, local and regional recurrence and the possibility of multiple primary tumors due to field cancerization from carcinogen exposure [3–5]. Despite advances in imaging, surgery and multimodality therapy, there has been only modest improvement of approximately 15 % in survival over the past 50 years. Globally, the 5-year survival rate is 60 % [6]. Tobacco use and alcohol consumption are often associated with the development of oral SCC; however, infection with certain strains of human papilloma virus is rapidly becoming a major cause of this disease, especially in the oropharynx [7, 8].

Oral SCC is a debilitating disease often associated with detrimental impact on quality of life. However, early detection and treatment may reduce the side effects of the disease and improve prognosis. Unfortunately, only 30–40 % of oral SCC patients present with early stage disease [9]. Many patients do not have symptoms or present to their physician until their lesions are large and advanced.

Traditional detection and staging of oral SCC includes directed biopsies after physical examination, endoscopy, and imaging studies such as computed tomography (CT), magnetic resonance (MRI), and positron emission tomography (PET) with 2-deoxy-2-[^{18}F]fluoro-$_D$-glucose (^{18}F-FDG) [10]. However, each imaging technique has limitations, especially in resolution and the sensitivity to detect small lesions.

There is a critical need to develop novel imaging technologies and therapeutics to detect and treat cancers at an early stage. Superficial lesions are notoriously difficult to image with CT or MRI. ^{18}F-FDG PET in the head and neck is typically described as demonstrating the capability to detect tumors of 1 cm^3 in volume, although the detection limit varies depending upon the metabolic uptake of the tumor [11]. Additionally, the high glucose utilization of the tonsillar tissue in the pharynx may complicate the image analysis of adjacent structures. Centers such as ours that perform large volumes of skull base surgery have experienced challenges with traditional ^{18}F-FDG PET imaging of tumors of the sinonasal tract, nasopharynx, and skull base due to their proximity to the high glucose-utilizing tissue of the brain. Due to its high sensitivity, PET has the potential to detect small lesions in regions with low background activity.

While ^{18}F-FDG is the gold standard radiotracer for clinical use, novel tracers such as ^{64}Cu-liposomes possess characteristics that may be beneficial in this patient population. ^{64}Cu-liposomes are unique and multifunctional as they can act as a radiotracer probe for cancerous lesions, can be used as a method to assess the accumulation of nanoparticles within lesions, and can be used as a vehicle for targeted drug delivery. ^{64}Cu-liposomes have been utilized for PET imaging in preclinical models of breast cancer and cardiovascular disease [12–17]. ^{64}Cu has a 12.7-h half-life and can be conjugated to 100-nm liposomes [13, 14]. These nanoparticles are excluded in normal tissues based on vascular permeability, but malignant tumors disproportionately accumulate these liposomes based on the enhanced permeability and retention effect [18]. The ability to conjugate specific targeting ligands to

the liposome surface and to enclose therapeutic drugs within the particle facilitates their use both as an imaging agent and a potential targeted therapeutic agent [19]. Previous studies have validated the liposomal distribution obtained by PET imaging with optical microscopy using the liposomal core to carry the fluorescent tracer or by comparison with other large tracers such as albumin [12, 15, 16, 20].

The hamster model of head and neck cancer has been shown to be an effective model of the transition from premalignant to fully malignant lesions [5, 21, 22]. In this study, we compare PET imaging with ^{64}Cu-liposomes and ^{18}F-FDG to assess the future potential for imaging and drug delivery in the established hamster model of oral SCC across all pathologic stages from early precancerous lesions to carcinoma. We set out to determine if ^{64}Cu-liposomes would accumulate in precancerous lesions as well as in invasive oral SCC of the head and neck.

Materials and Methods

Overview of the Study

In total, four treatment groups (six animals in each group, Table 1) were studied. Two groups were imaged 5–8 weeks after the start of 7,12-dimethylbenz[a]anthracene (DMBA) application, representing early precancerous lesions. Another two groups were imaged between 12 and 22 weeks after the start of DMBA application, representing late, pathologically advanced lesions. In each pair of groups, DMBA application was halted 1 to 2 weeks prior to PET in one cohort.

For each animal, PET images were acquired with both ^{18}F-FDG and ^{64}Cu-liposomes (Supplemental Fig. 1), within 1 week of each other. After the last PET time point, cheek pouches were harvested and sent for histological analysis. Margin-marking dye was placed on the sample after harvest and was used to determine orientation of histology samples for better correlation with PET images.

Tumor Induction

All animal experiments were conducted under a protocol approved by the University of California, Davis, Animal Care and Use Committee (Davis, CA). Four to five week-old male golden Syrian hamsters (Harlan, Indianapolis, IN) weighing ~150 g were studied due to the large buccal mucosa surface area and the well-established protocol for inducing squamous neoplasms [23]. In addition, DMBA-induced tumors follow the pathological changes associated with human oral cavity tumors [24]. Animals were housed in a temperature-controlled room in ventilated cages and maintained on a 12-h day/night cycle with animal diet and water provided *ad libitum*. Tumors were induced in the buccal pouch by topical application of 20 μl of 0.5 or 2.5 % (grams per milliliter) of the DMBA (Sigma-Aldrich, St. Louis, MI) in mineral oil three times a week for 5–22 weeks. Animals received DMBA applications either bilaterally (right and left cheek pouches) or unilaterally (right cheek pouch only). In an effort to control for inflammation and its potential for false-positive scans, DMBA application was stopped for up to 2 weeks prior to PET imaging in a subset of cases.

Lesion Grading by Gross Examination of Mucosa

Throughout the DMBA application process, animals were visually inspected weekly for signs of mucosal change (Supplemental Fig. 2). Animals were classified as having early precancerous lesions when gross examination of the mucosa showed reddened, thick, and scaly patches, characteristic of hyperkeratosis. White and raised lesions less than 1 mm in diameter were also included in the precancerous group and were generally observed early in

the DMBA application process of 5–8 weeks. Raised, reddened lesions >2 mm in diameter were classified as late, more pathologically advanced lesions. These were generally observed at ~12–21 weeks after the start of DMBA application.

Synthesis of the Radioactive Tracers

^{18}F-FDG and $^{64}CuCl_2$ were purchased from PETNET (PETNET Solutions, Sacramento, CA) and MIR Radiological Science at Washington University Medical School (St. Louis, MI), respectively, under a protocol controlled by the University of California, Davis.

^{64}Cu-liposome preparation followed a previously reported method [13]. All lipids and a mini-extruder were purchased from Avanti Polar Lipids (Alabaster, AL). In brief, lipids (approximately 25 mg, HSPC/cholesterol/DSPE-PEG2K-OMe/6-BAT-PEG-lipid=55.5:39:5.0:0.5, mol/mol/mol/mol) in chloroform were added to a glass test tube. The solvent was evaporated by gently blowing nitrogen gas under a low spinning vortexer to create a thin film. After additional drying for at least 4 h in the lyophilizer, lipids were resuspended in 0.1 M ammonium citrate buffer (0.4 ml, pH 5.5), and a glass test tube was then incubated in the water bath for 5–10 min at 60 °C. The milky solution was drawn into the syringe and extruded 21 times through a 100-nm membrane filter (Whatman, NJ) on a 60–62 °C heating block. After cooling to room temperature, ^{64}Cu (18.5 MBq/3 mg total lipids) was added to the liposomes in 0.1 M ammonium citrate (0.1 ml) buffer. After incubation at 30 °C for 1 h, 0.1 M EDTA (20 μl) was added and incubated for 10 min in order to remove nonspecifically bound ^{64}Cu. ^{64}Cu-liposomes were purified using a size exclusion column filled with G75 in PBS (1×). The radiochemical purity of liposomes on TLC was more than 95 %. Averaged specific activity through several studies was 5.7±0.5 MBq/mg.

PET Imaging

All PET images were obtained on a microPET-Focus 120 (Siemens Medical Solutions, USA, Inc.). Each group of animals underwent ^{18}F-FDG and ^{64}Cu-liposome PET imaging during the same week or within 1 week of each other.

^{18}F-FDG Protocol

The animals were anesthetized with 2–3 % isoflurane, and ^{18}F-FDG was administered by intravenous (IV) injection. After 30 min, the animals were again anesthetized with 2–3 % isoflurane and placed individually in the supine position on the PET scanner bed. Static PET scans were then obtained for 30 min.

^{64}Cu-liposome Protocol

Animals were anesthetized with 2–3 % isoflurane and placed individually in the supine position on the scanner bed. Thirty-minute PET acquisitions were started immediately after IV injection of the ^{64}Cu-liposomes and again at 24 h postinjection.

Image Analysis

Images were obtained using the ASI Pro Virtual Machine Software (CTI Molecular Imaging), reconstructed using a maximum *a posteriori* algorithm, and quantified with ASI Pro by defining regions of interest (ROI) and calculating the percent injected dose per cubic centimeter (%ID/cc) within the ROIs.

Histopathology Examination and Lesion Grading

After the last time point of PET imaging, the animals were euthanized, and the cheek pouches were removed, fixed overnight in 10 % formalin and then placed in 70 % ethanol.

After fixation, tumors were processed with a Tissue Tek VIP then paraffin embedded using a Tissue Tek TEC (Sakura Finetek, Torrance, CA, USA). Four-micron slices were cut using a manual rotary microtome (Leica RM2235, Leica Microsystems Inc., Bannockburn, IL USA) and stained with hematoxylin and eosin.

All samples were examined by a pathologist blinded to the study. Tissue sections were evaluated for oral epithelial dysplasia based on the presence of architectural and cytological changes according to the WHO classification [25]. Lesions were subclassified into one of four categories including mild dysplasia (MD), severe dysplasia (SD), carcinoma *in situ* (CIS), and SCC. *MD* demonstrates proliferation of cells of the basal and parabasal layers which do not extend beyond the lower third of the epithelium. Cytological atypia is generally mild, and mitoses, when present, are usually basally located and normal. Architectural changes are minimal. In *SD*, there is an abnormal proliferation extending from the basal layer into the upper third of the epithelium. Cytological and architectural changes can be very prominent. *CIS* is characterized by full-thickness cytological and architectural changes. Cases were classified as *SCC* when there was invasion into the underlying connective tissue.

The degree of acute inflammation in each sample was also evaluated in the stromal area adjacent to the lesion. Acute inflammatory cells (PMNs) were counted at 40× magnification, and the degree of inflammation was scored as either 0, 1+, 2+ or 3+ based on counting either 0, 1–10, 11–20 or more than 20 inflammatory cells, respectively. Areas selected for counting of PMNs were limited to the stroma underlining the lesion and were devoid of necrosis or cellular degeneration. We avoided counting the PMNs in areas adjacent to ulcerated lesions.

Statistical Analysis

All statistical analyses were performed using software: Excel 11.0 (Microsoft, Seattle, WA), and MiniTab 16 (Minitab Inc., State College, PA). Data were recorded as a mean ± standard deviation for continuous data. Significant differences were assessed using a two-tailed Student's *t* test (for individual comparisons) and ANOVA (for multiple comparisons), with a *P* value less than 0.05 indicating a statistically significant difference.

Results

Pathological grade and corresponding level of inflammation were assessed from histopathology samples across all animal groups (Fig. 1). This model reliably produced pathologies ranging from MD to SCC. Lesions graded as pathologically normal and those reflective of MD were found only in early lesion groups that received DMBA application for 5 or 8 weeks, while more pathologically advanced lesions graded as SD, CIS, and SCC were found in groups that were treated with DMBA for a longer time period. Highest levels of inflammation (3+) were observed in lesions graded as SCC, while all other pathology grades had inflammation levels ranging from 0 to 2+.

Unilateral, right-sided DMBA application resulted in tumors in the right cheek pouch only, showing no evidence of pathology on the contralateral cheek pouch that did not receive DMBA treatment (Fig. 2a). In these animals, the untreated left side served as an internal normal mucosal control. Bilateral DMBA application resulted in bilateral tumors confirmed by PET images and histopathology of tissue sections (data not shown). Lesions observed in the PET images were compared with their corresponding histopathology in panels b, c, d, and e of Fig. 2 for normal tissue, MD, CIS, and SCC, respectively.

PET images obtained with ^{18}F-FDG and with ^{64}Cu-liposome imaging at 0 and 24 h demonstrate the differences between the tracers and differences between the treated and

untreated animals for each of the four DMBA-treated groups (Fig. 3). The images are normalized to the blood signal for ^{64}Cu-liposomes and to the heart muscle for ^{18}F-FDG PET scans in order to improve visualization. No lesions were detected in images obtained with either radioisotope in the untreated animal (column a). Groups that received DMBA application for 5 and 8 weeks had lesions classified as early precancerous lesions and were pathologically graded as normal to MD. Figure 3 shows an example of one animal from each of the 5-week (column b) and 8-week (column c) DMBA-treated groups. In these two animals, lesions are clearly visualized at 24 h post-^{64}Cu-liposome injection (arrows) and are not visible following imaging with ^{18}F-FDG. A subset of early lesions graded as MD within these two groups (4 lesions/18 cheek pouches) were detected only with ^{64}Cu-liposome imaging at 24 h postinjection and were not detected with ^{18}F-FDG (images not shown). Groups that received DMBA application for 22 weeks (column d) and 12 weeks (column e) have lesions classified as late pathologically advanced lesions graded from normal to SCC (normal grades are from untreated control animals or untreated contralateral cheek pouches). All lesions pathologically graded as SD, CIS, and SCC were detected with both ^{64}Cu-liposome and ^{18}F-FDG imaging at 22 and 12 weeks.

^{64}Cu-liposomes circulated stably within the blood pool (Fig. 4). Across all animals, the average circulating activity decreased from 10.2±2.4 %ID/cc at the time of the injection to 3.8±1.4 %ID/cc at 24 h postinjection (P<0.001). Clearance of ^{18}F-FDG from the blood occurs more rapidly and cannot be directly estimated from the cardiac PET images at the 30-min imaging time point. ^{18}F-FDG activity within the heart muscle (corresponding to the peak uptake of ^{18}F-FDG in the lesions) averaged 2.6±0.6 %ID/cc across all animals at the 30-min time point and was significantly lower as compared to radioactivity resulting from^{64}Cu-liposomes at 24 h postinjection (P<0.001).

Averaged across all animals, the accumulation of ^{64}Cu-liposomes within lesions increased from 0 h (1.2±0.4 %ID/cc) to 24 h (3.5±1.4 %ID/cc; P<0.001) (Fig. 5a). At 24 h postinjection (approximately corresponding to the peak accumulation), ^{64}Cu-liposome activity exceeded the averaged accumulation at the 30-min time point (peak accumulation) of ^{18}F-FDG (1.4±0.8 %ID/cc) (P<0.001). A similar trend was observed within each individual group (Fig. 5b); the accumulation of ^{64}Cu-liposomes at 24 h exceeded the accumulation of ^{64}Cu-liposomes at 0 h and of ^{18}F-FDG in each group (P<0.05).

To study the effect of stopping DMBA application on the images and tracer accumulation, a comparison was performed between the cases where DMBA was stopped before PET imaging and the cases where DMBA was not stopped (Fig. 5c). No significance was reached for each radioisotope, suggesting that ^{18}F-FDG and ^{64}Cu-liposome accumulation was not significantly altered by stopping DMBA application before PET. Also, ^{64}Cu-liposome accumulation was similar in lesions graded as low inflammation (0–1) and high inflammation (2–3) (Fig. 5c).

Tumor ROIs were then grouped according to their graded histopathology categories (Fig. 5d). As the disease progressed from normal (no treatment contralateral control) to SCC, the accumulation of both radiotracers increased: ^{18}F-FDG from 0.3±0.1 to 2.5±1.0 %ID/cc, ^{64}Cu-liposomes at the 0-h time point from 0.2±0.1 to 1.5±0.4 %ID/cc, and ^{64}Cu-liposomes at 24 h after injection from 0.4±0.2 to 4.3±1.0 %ID/cc. With the exception of CIS and SCC, peak ^{64}Cu-liposome accumulation (^{64}Cu-liposome, 24 h) was greater than that obtained with ^{18}F-FDG for all other pathological states (P<0.05).

The lesion-to-brain ratio also demonstrated improved imaging characteristics for ^{64}Cu-liposomes (Fig. 6a, b), compared with ^{18}F-FDG. When grouped according to DMBA application pattern (Fig. 6a), the lesion-to-brain ratio of ^{18}F-FDG (0.2±0.1 to 1.0±0.7) was

significantly lower than that of ^{64}Cu-liposomes at 24 h after injection (4.9±2.1 to 7.1±1.1; $P<0.001$) in each group. When grouped according to the lesion histopathology (Fig. 6b), the lesion-to-brain ratios increased with the progress of the lesion from normal tissue to SCC for ^{18}F-FDG and for ^{64}Cu-liposomes at 0 and 24 h after injection. Within each grade, ^{18}F-FDG showed significantly smaller lesion-to-brain ratios than ^{64}Cu-liposomes at 24 h after injection ($P<0.01$). The lesion-to-brain ratio was higher at 24 h after the injection of ^{64}Cu-liposomes, as compared to the 0-h time point ($P<0.01$).

Similarly, the lesion-to-cheek pouch background ratio was calculated as a measurement of imaging sensitivity (Fig. 6c, d). ^{64}Cu-liposome accumulation at 24 h postinjection ranged from 7.1±3.4 to 15.4±7.6, while ^{18}F-FDG accumulation ranged from 3.0±1.4 to 7.0±1.6 ($P<0.05$, except the 12-week 2.5 % treatment group). When grouped according to their graded histopathology categories, lesion-to-cheek pouch background ratios are higher for ^{64}Cu-liposomes at 24 h than ^{18}F-FDG except in the SD and CIS groups ($P<0.05$).

Discussion

Early detection of neoplasms offers the potential for higher cure rates and decreased treatment-related morbidity. Taken together, our data demonstrate the increased sensitivity of ^{64}Cu-liposomes for detecting abnormal mucosa and the potential to improve the detection of early tumors compared to ^{18}F-FDG, which typically has a 1-cm^3 size limit for detection. While we have demonstrated that the accumulation is not restricted to neoplasms, the greater sensitivity of ^{64}Cu-liposomes improves our ability to detect early dysplastic or preneoplastic lesions not visualized on ^{18}F-FDG images. By detecting abnormal tissue earlier, treating physicians will be alerted to high-risk areas allowing earlier biopsy and management. This increased sensitivity occurs at the expense of specificity for malignancies. Sampled tissue showing mild mucosal changes (histologically normal and mild dysplasia) demonstrated increased ^{64}Cu-liposome uptake compared to nontreated adjacent tissue. There are several possible explanations for this finding. Topical application of the DMBA carcinogen in this model leads to tissue changes including inflammation in advance of neoplastic transformation [26]. This inflammation results in leaky capillaries allowing the liposomes to exit the vasculature and accumulate in the tissues [27]. Our finding that a period without carcinogen exposure prior to imaging did not influence radiotracer accumulation would suggest that this is unlikely to be the sole explanation. Another possibility is that we are detecting neoplastic transformation before a definitive histopathological diagnosis can be determined. This is an interesting and important possibility as oral cancers and head and neck neoplasms are often associated with large field carcinogen exposure from tobacco smoke and alcohol ingestion [28]. After appropriate surgical resection, it is not uncommon for second malignancies to develop despite negative surgical margins by histopathology. Genetic analysis of adjacent histologically “normal” tissue has demonstrated mutations well beyond the cleared margins of the tumor [29]. Therefore, we may be imaging preneoplastic transformations with ^{64}Cu-liposomes earlier than the lesions would be detected with traditional histopathology. Future studies analyzing the genetic alterations found in ^{64}Cu-liposome-positive, histopathologically normal lesions would help to answer this question.

An additional advantage of ^{64}Cu-liposomes compared to ^{18}F-FDG is the dramatically increased lesion-to-brain ratio. While pure skull base tumors are rare, tumors of the oral cavity and pharynx may extend to the skull base and travel along nerves toward the brain. While MRI and CT imaging provide excellent anatomical imaging, postradiation edema and scarring can be difficult to distinguish from recurrent tumor. As such, functional imaging is often a useful adjunct to evaluate these lesions. As the brain is an obligate glucose-metabolizing organ, decreasing the brain background by using an alternative tracer to the glucose analog FDG dramatically improves the lesion detection with PET imaging in this

anatomic location, offering the potential to increase both sensitivity and specificity in imaging tumors near the brain. Similarly, the tonsillar tissue in the oropharynx may have a high glucose uptake and background FDG accumulation. ^{64}Cu-liposomes may also improve our imaging of lesions in this critical area as well.

Beyond the use of ^{64}Cu-liposomes for lesion detection, the results presented here demonstrate the opportunity for liposomal drug delivery in such lesions. Our radiolabeling technique allows for the facile labeling of liposomes that contain a therapeutic cargo, and we have previously demonstrated that for a stable liposomal formulation, the biodistribution of the radioactive liposomal shell is similar to that of the liposomal cargo [13, 20, 30]. The accumulation of ^{64}Cu-liposomes (%ID/cc) was significantly higher at 24 h than with ^{18}F-FDG, where an accumulation of 2.6–4.14 %ID/cc of ^{64}Cu-liposomes was observed in lesions in this study. This compares favorably to other studies of radiotracer accumulation in similar-sized animal models, and demonstrates the possibility of utilizing this model to study drug delivery to head and neck tumors in the future [31]. The selective accumulation in these tumors allows for dramatic improvement in the therapeutic ratio of drug delivery to the tumor compared to drug delivery to normal tissues. While we did observe enhanced accumulation in both cancerous and precancerous tissues, the opportunity to concentrate therapeutics in early lesions may prove valuable in cancers that have a high likelihood of local recurrence. In such cancers, a combination of precancer and advanced disease exists simultaneously, and such early treatment may reduce progression. More importantly, it offers the potential to increase the therapeutic efficacy while minimizing systemic toxicity. Future studies will address the application of this concept.

Conclusion

^{64}Cu-liposomes accumulate in abnormal mucosa in the hamster DMBA-induced oral carcinogenesis model. When compared to traditional ^{18}F-FDG PET, ^{64}Cu-liposomes demonstrated increased sensitivity and earlier detection. Specificity to cancer was reduced in this model with early, histologically normal and dysplastic lesions being identified as well. Accumulation of the ^{64}Cu-liposomes was significant and offers the potential for both novel imaging and therapeutic applications of this tracer.

Supplementary Material

Refer to Web version on PubMed Central for supplementary material.

Acknowledgments

Funding was provided by NIHR01CA103828 and NIHR01CA134659.

References

1. Saman DM. A review of the epidemiology of oral and pharyngeal carcinoma: update. Head Neck Oncol. 2012; 4:1. [PubMed: 22244087]
2. Leemans CR, Braakhuis BJ, Brakenhoff RH. The molecular biology of head and neck cancer. Nat Rev Cancer. 2011; 11:9–22. [PubMed: 21160525]
3. Kesting MR, et al. Results of esophagogastroduodenoscopy in patients with oral squamous cell carcinoma—value of endoscopic screening: 10-year experience. Int J Oral Maxillofac Surg. 2009; 67:1649–1655.
4. Yang Y, Ge JP, Zhou ZT. Effects of thalidomide on DMBA-induced oral carcinogenesis in hamster with respect to angiogenesis. J Oral Pathol Med. 2009; 38:455–462. [PubMed: 19141066]

5. Farwell DG, et al. Time-resolved fluorescence spectroscopy as a diagnostic technique of oral carcinoma validation in the hamster buccal pouch model. Arch Otolaryngol Head Neck Surg. 2010; 136:126–133. [PubMed: 20157056]
6. NIH. Bethesda, MD: National Institute of Dental and Craniofacial Research; 2011. Oral cancer 5-year survival rates by race, gender, and stage of diagnosis. http://www.nidcr.nih.gov/datastatistics/finddatabytopic/oralcancer/oralcancer5yearsurvivalrates.htm. [Accessed 8 July 2013]
7. Chaturvedi AK, Engels EA, Anderson WF, Gillison ML. Incidence trends for human papillomavirus-related and -unrelated oral squamous cell carcinomas in the United States. J Clin Oncol. 2008; 26:612–619. [PubMed: 18235120]
8. Chaturvedi AK, et al. Human papillomavirus and rising oropharyngeal cancer incidence in the United States. J Clin Oncol. 2011; 29:4294–4301. [PubMed: 21969503]
9. Goon PK, et al. HPV & head and neck cancer: a descriptive update. Head Neck Oncol. 2009; 1:36. [PubMed: 19828033]
10. Al-Ibraheem A, Buck A, Krause BJ, Scheidhauer K, Schwaiger M. Clinical applications of FDG PET and PET/CT in head and neck cancer. J Oncol. 2009; 2009:208725. [PubMed: 19707528]
11. Yamazaki Y, et al. Assessment of cervical lymph node metastases using FDG-PET in patients with head and neck cancer. Ann Nucl Med. 2008; 22:177–184. [PubMed: 18498032]
12. Zhang H, et al. Dynamic imaging of arginine-rich heart-targeted vehicles in a mouse model. Biomaterials. 2008; 29:1976–1988. [PubMed: 18255141]
13. Seo JW, Zhang H, Kukis DL, Meares CF, Ferrara KW. A novel method to label preformed liposomes with (CU)-C-64 for positron emission tomography (PET) imaging. Bioconjugate Chemistry. 2008; 19:2577–2584. [PubMed: 18991368]
14. Seo JW, et al. Liposomal Cu-64 labeling method using bifunctional chelators: poly(ethylene glycol) spacer and chelator effects. Bioconjugate Chemistry. 2010; 21:1206–1215. [PubMed: 20568726]
15. Rygh CB, et al. Longitudinal investigation of permeability and distribution of macromolecules in mouse malignant transformation using PET. Clin Cancer Res. 2011; 17:550–559. [PubMed: 21106723]
16. Watson KD, et al. Ultrasound increases nanoparticle delivery by reducing intratumoral pressure and increasing transport in epithelial and epithelial-mesenchymal transition tumors. Cancer Res. 2012; 72:1485–1493. [PubMed: 22282664]
17. Wong AW, et al. A comparison of image contrast with (64)Cu-labeled long circulating liposomes and (18)F-FDG in a murine model of mammary carcinoma. Am J of Nucl Med and Mol Imag. 2013; 3:32–43.
18. Torchilin VP. Recent advances with liposomes as pharmaceutical carriers. Nat Rev Drug Discov. 2005; 4:145–160. [PubMed: 15688077]
19. Gabizon A, Shmeeda H, Horowitz AT, Zalipsky S. Tumor cell targeting of liposome-entrapped drugs with phospholipid-anchored folic acid-PEG conjugates. Adv Drug Deliver Rev. 2004; 56:1177–1192.
20. Paoli EE, et al. An optical and microPET assessment of thermally-sensitive liposome biodistribution in the Met-1 tumor model: importance of formulation. J Contr Release. 2010; 143:13–22.
21. Sun Y, et al. Fluorescence lifetime imaging microscopy: *in vivo* application to diagnosis of oral carcinoma. Opt Lett. 2009; 34:2081–2083. [PubMed: 19572006]
22. Meier JD, et al. Time-resolved laser-induced fluorescence spectroscopy as a diagnostic instrument in head and neck carcinoma. Otolaryng Head Neck. 2010; 142:838–844.
23. Shklar G. Experimental oral pathology in the Syrian hamster. Progr Exp Tumor Res. 1972; 16:518–538. [PubMed: 4557243]
24. Manoharan S, Vasanthaselvan M, Silvan S, Baskaran N, Kumar Singh A, Vinoth Kumar V. Carnosic acid: a potent chemopreventive agent against oral carcinogenesis. Chem Biol Interact. 2010; 188:616–622. [PubMed: 20816777]
25. Thompson L. World Health Organization classification of tumours: pathology and genetics of head and neck tumours. Ear Nose Throat J. 2006; 85:74. [PubMed: 16579185]

26. Manoharan S, Balakrishnan S, Menon VP, Alias LM, Reena AR. Chemopreventive efficacy of curcumin and piperine during 7,12-dimethylbenz [a]anthracene-induced hamster buccal pouch carcinogenesis. Singap Med J. 2009; 50:139–146.

27. Maruyama K. Intracellular targeting delivery of liposomal drugs to solid tumors based on EPR effects. Adv Drug Deliv Rev. 2011; 63:161–169. [PubMed: 20869415]

28. Morris LG, Sikora AG, Patel SG, Hayes RB, Ganly I. Second primary cancers after an index head and neck cancer: subsite-specific trends in the era of human papillomavirus-associated oropharyngeal cancer. J Clin Oncol: official journal of the American Society of Clinical Oncology. 2011; 29:739–746.

29. Poh CFZL, Anderson DW, Durham JS, Williams PM, Priddy RW, Berean KW, Ng S, Tseng OL, MacAulay C, Rosin MP. Fluorescence visualization detection of field alterations in tumor margins of oral cancer patients. Clin Cancer Res. 2006; 12:6716–6722. [PubMed: 17121891]

30. Qin S, Seo JW, Zhang H, Qi J, Curry FR, Ferrara KW. An imaging-driven model for liposomal stability and circulation. Mol Pharm. 2010; 7:12–21. [PubMed: 19621944]

31. Oku N, et al. PET imaging of brain cancer with positron emitter-labeled liposomes. Int J Pharm. 2011; 403:170–177. [PubMed: 20934495]

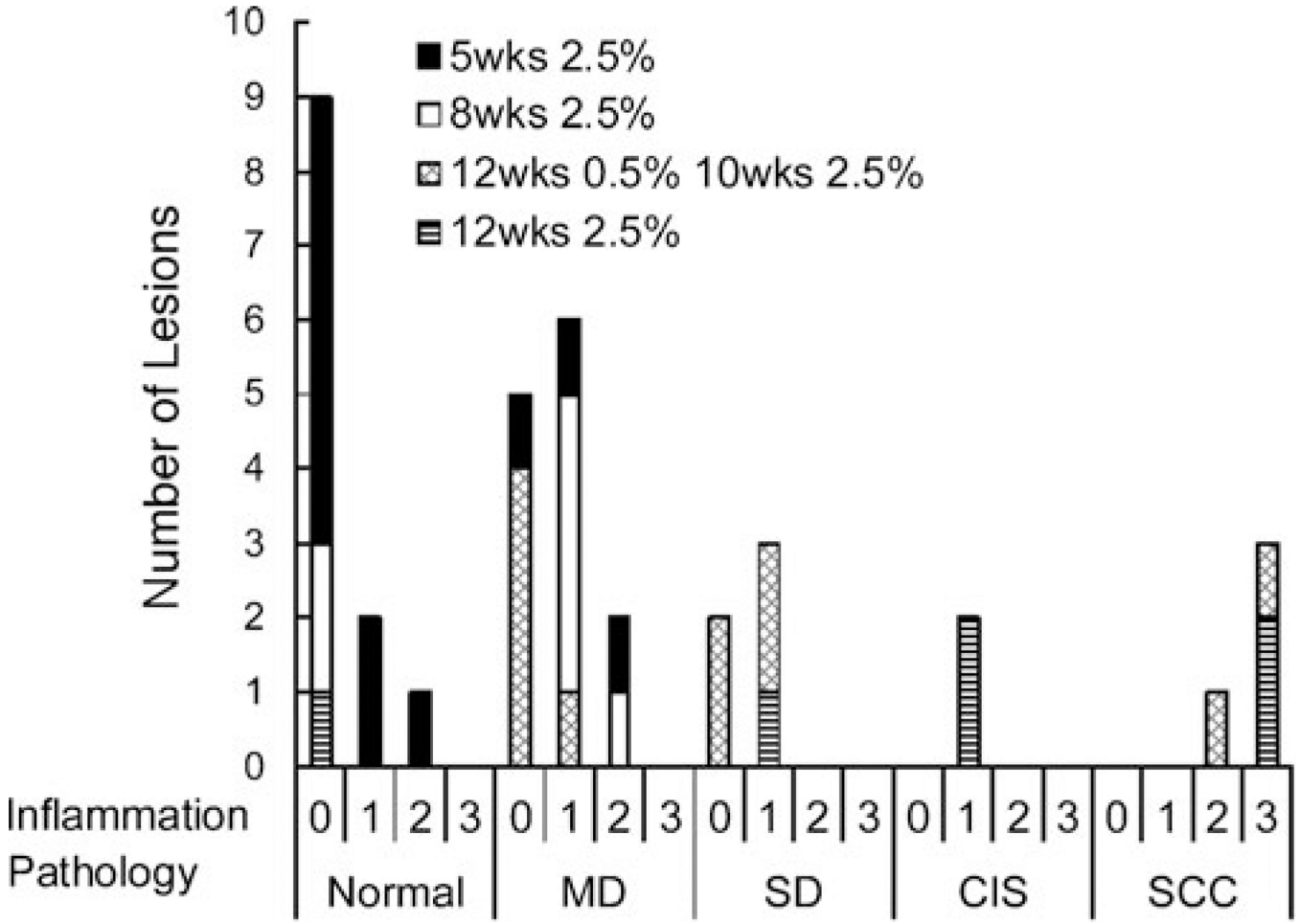

Fig. 1.
Total number of lesions across all DMBA-treated groups as a function of disease state and associated inflammation score.

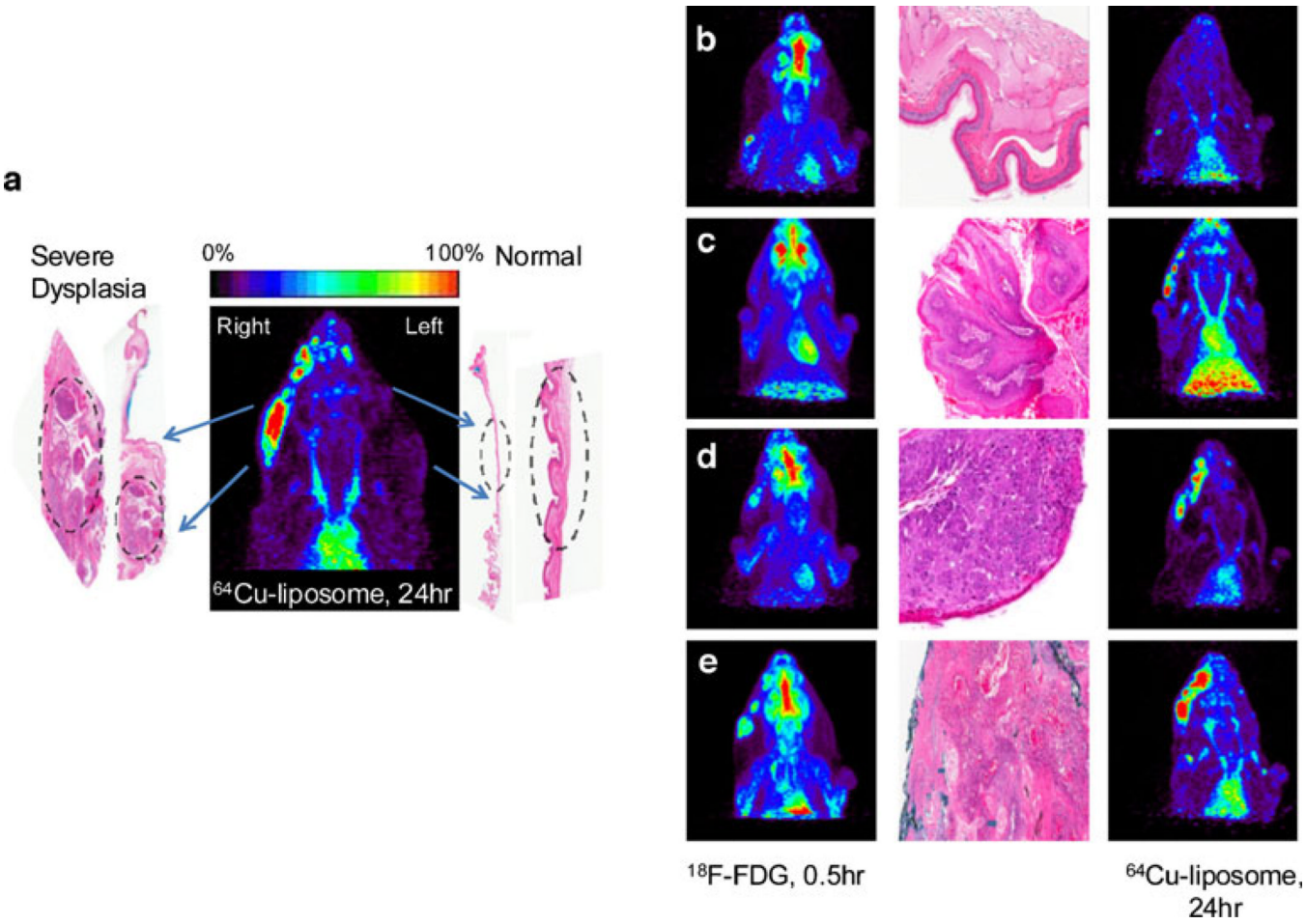

Fig. 2.

Correlative PET and histology images. **a** DMBA painting on the right cheek pouch only resulting in severe dysplasia, while the left cheek pouch did not receive DMBA treatment and demonstrated normal epithelium. ^{64}Cu-liposome PET image (24 h) showing difference in radioactive accumulation between the sides of the cheek pouch. **b–e** ^{18}F-FDG images (*left*), histological images (*middle*) and ^{64}Cu-liposome images (24 h) (*right*) for different disease stages: **b** normal (nontreated) control; **c** MD; **d** SD; **e** SCC.

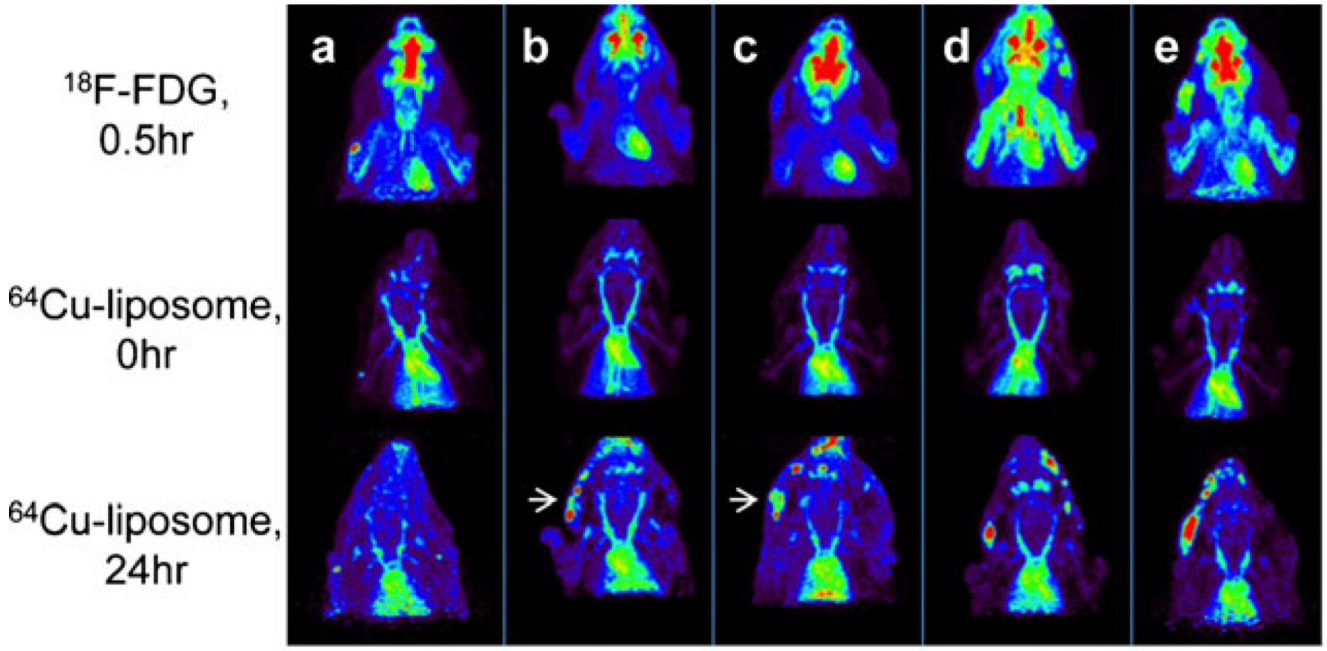

DMBA application	No treatment	5wks 2.5% Continual	8wks 2.5% Stopped	12wks 0.5% 10wks 2.5% Continual	12wks 2.5% Stopped
Pathology grading	Normal	Normal - MD	Normal - MD	Normal - SCC	Normal - SCC

Fig. 3.

Typical ^{18}F-FDG (*upper*) and ^{64}Cu-liposome images at 0 h (*middle*) and at 24 h (*lower*) for hamsters with no treatment (**a**), treated with DMBA for 5 weeks at 2.5 % (**b**), 8 weeks at 2.5 % (**c**), 12 weeks at 0.5 %, followed by 10 weeks at 2.5 % (**d**), and 12 weeks at 2.5%(**e**). The images are normalized with the radioactivity in the heart muscle (^{18}F-FDG) and heart chamber blood activity (^{64}Cu-liposomes). *White arrows* indicate lesions in early disease groups detected in ^{64}Cu-liposome images (24 h), but not detected in ^{18}F-FDG images. A high brain uptake of the radioactivity was also observed in ^{18}F-FDG, but not in ^{64}Cu-liposome, images.

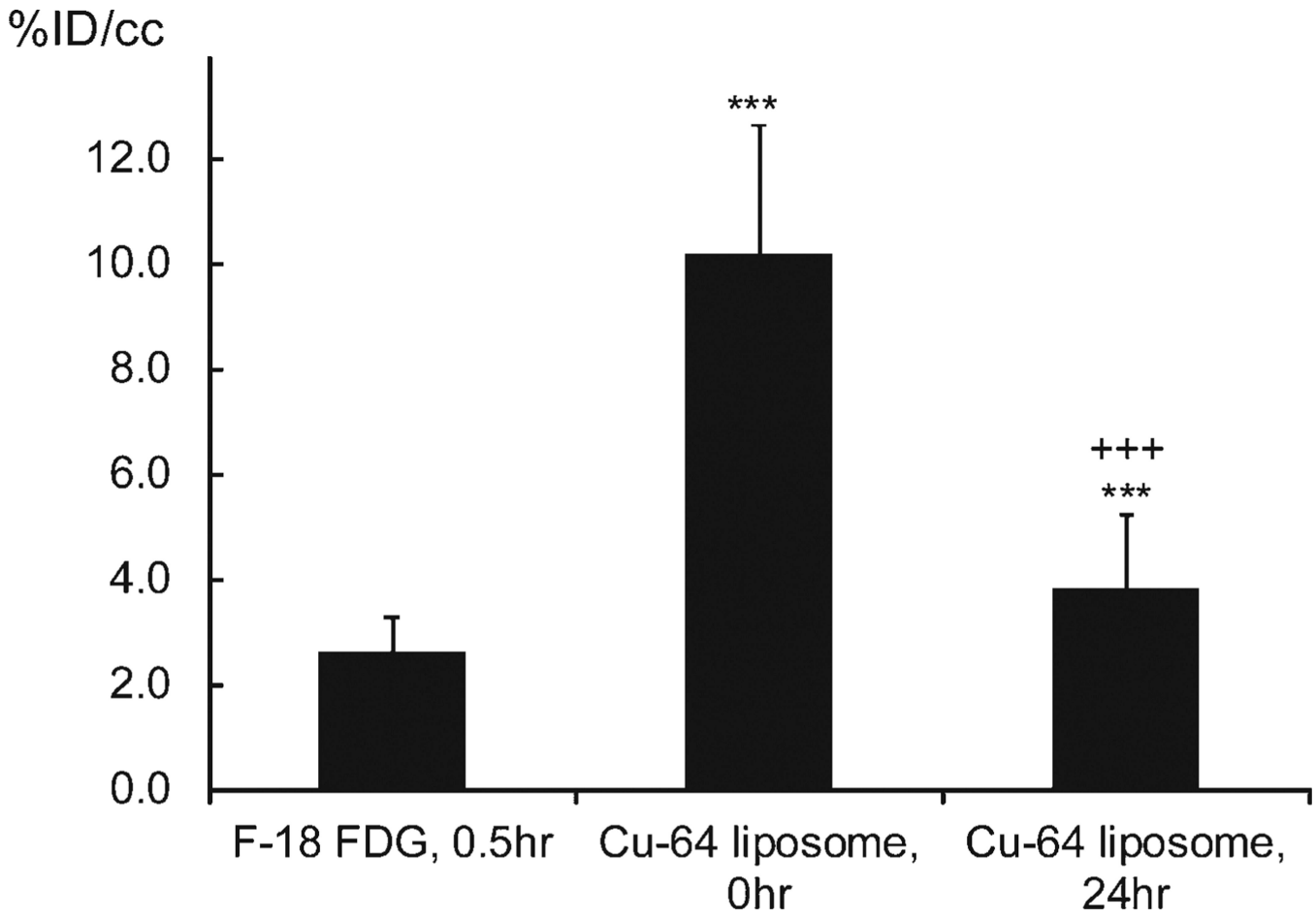

Fig. 4.

Radioactivity in the heart muscle (^{18}F-FDG) and heart chamber blood (^{64}Cu-liposomes). Statistical significances are shown: *asterisk*, ^{18}F-FDG vs ^{64}Cu-liposomes; *plus sign*, ^{64}Cu-liposomes 0 vs 24 h; *single symbol*, $p < 0.05$; *double symbols*, $p < 0.01$; *triple symbols*, $p < 0.001$.

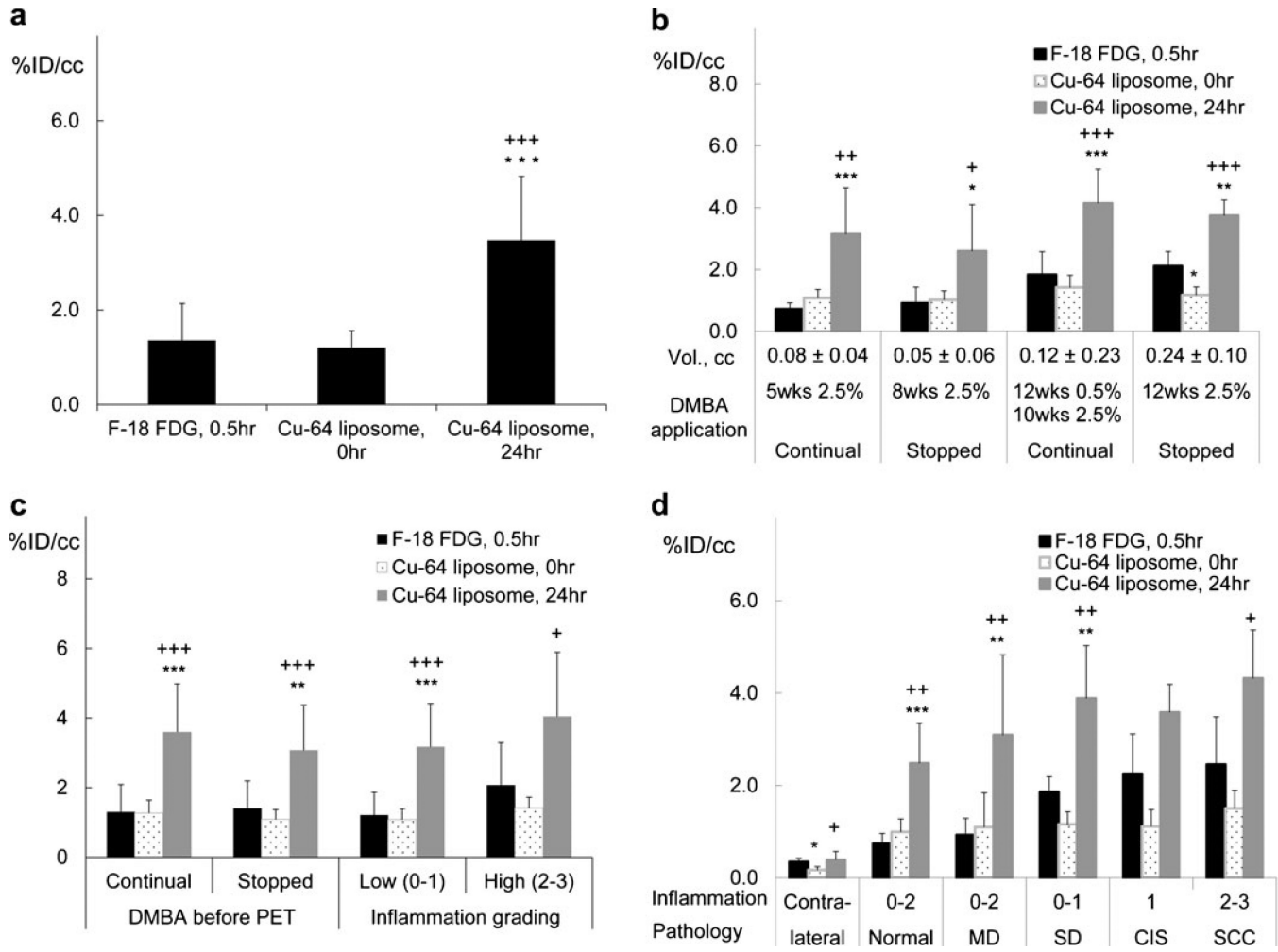

Fig. 5.

Radioactive accumulation in lesions imaged with ^{18}F-FDG (30min) and ^{64}Cu-liposomes (0 and 24 h): **a** for all animals (no grouping); **b** grouped by different DMBA application patterns; **c** grouped according to continuous or halted DMBA application; **d** grouped by inflammation and pathological conditions. For each case, radioactivity accumulated within the lesion was greater with ^{64}Cu-liposomes than with ^{18}F-FDG at the respective peak time points. Statistical significance is shown as follows: *asterisk*, ^{18}F-FDG vs ^{64}Cu-liposomes; *plus sign*, ^{64}Cu-liposomes 0 vs 24 h; *single symbol*, $p < 0.05$; *double symbols*, $p < 0.01$; *triple symbols*, $p < 0.001$.

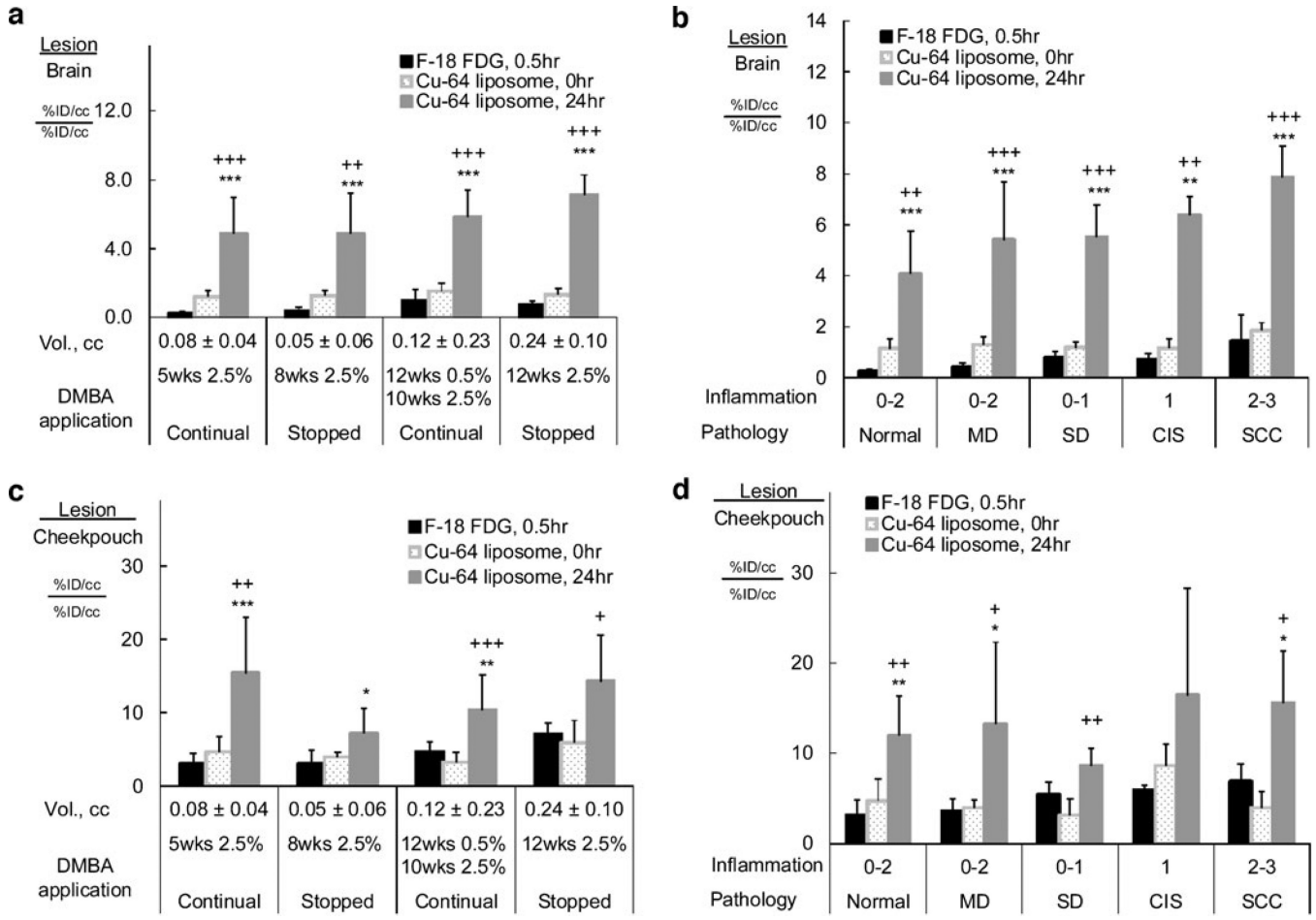

Fig. 6.

The ratios of accumulation in lesion vs brain (**a** and **b**) and lesion vs cheek pouch background (**c** and **d**): **a** and **c**, grouped by DMBA application patterns; b and d, grouped by pathological grades. In each case, the lesion-to-brain or cheek pouch ratios are higher in ^{64}Cu-liposome 24-h images than in ^{18}F-FDG images. Statistical significance is shown as follows: *asterisk*, ^{18}F-FDG vs ^{64}Cu-liposomes; *plus sign*, ^{64}Cu-liposomes 0 vs 24 h; *single symbol*, $p < 0.05$; *double symbols*, $p < 0.01$; *triple symbols*, $p < 0.001$.

Table 1

Animal grouping information

Group	DMBA application				Lesion		PET imaging time (weeks)	
	Unilateral (U) or bilateral (B)	Concentration (20 μl, g/ml) (%)	Duration of application (weeks)	Continual or stopped before PET	Volume (cc)	Grading	^{18}F-FDG	^{64}Cu-liposomes
1	B	2.5	5	Continual	0.08±0.04	Normal–MD	5	5
2	U	2.5	8	Stopped	0.05±0.06	Normal–MD	9	10
3	U and B	0.5	12	Continual	0.12±0.23	Normal–SCC	22	21
		2.5	10					
4	U	2.5	12	Stopped	0.24±0.10	Normal–SCC	13	13